

## High-precision geo-referencing of UAS data with robotic total stations

Lucas Dammert<sup>1</sup>, Tomas Thalmann<sup>1</sup>, Florian Pöppel<sup>1</sup>, David Monetti<sup>2</sup>,  
Hans-Berndt Neuner<sup>1</sup>, Gottfried Mandlbürger<sup>1</sup>

<sup>1</sup> TU Wien, Department of Geodesy and Geoinformation, 1040 Vienna, Austria - lucas.dammert@tuwien.ac.at

<sup>2</sup> Skyability GmbH, GZO-Dienstleistungszentrum 5, 7011 Siegendorf, Austria

**Keywords:** Trajectory, Mapping, UAV, Sensor fusion.

### Abstract

Robotic Total Stations (RTS) allow the measurement of 3D positions of kinematic targets with high accuracy. They find wide applications for geo-referencing multisensor systems, but little focus has been put on the geo-referencing of Unmanned Aerial Systems (UAS) with RTS.

In this study, we geo-reference an Unmanned Laser Scanning (ULS) point cloud using an RTS and an Inertial Measurement Unit (IMU) without using GNSS positions. We thoroughly investigate the UAS trajectory measured by an RTS, using photogrammetric reference positions and a redundant trajectory from a second RTS. In addition, we evaluate the generated ULS point cloud against a reference point cloud acquired by Terrestrial Laser Scanning (TLS).

For our field test, we find that the UAS trajectory shows an average 3D difference of less than 13 mm compared to our reference data sets. The generated point cloud has an average absolute 3D normal distance of 9 mm to our TLS reference.

### 1. Introduction

Efforts to improve the accuracy of mobile mapping systems span a wide range of application fields, from agriculture (Paraforos et al., 2017) to robotics (Vaidis et al., 2023). Among the most prominent mobile mapping systems are Unmanned Aerial Systems (UAS). Consequently, the search for highly accurate UAS is of great importance. One of the major sources of uncertainty in the generation of 3D data with UAS is the trajectory. The introduction of alternative positioning sensors to GNSS allows the improvement of the trajectory accuracy and thus of the acquired 3D data. In addition, this enables Unmanned Laser Scanning (ULS) surveys in GNSS-denied areas. One alternative positioning sensor is a Robotic Total Station (RTS), a geodetic measurement instrument relying on a line-of-sight to measure distance and angles to obtain 3D coordinates of the target. RTS operate at the lower millimetre accuracy for static applications with distances below 100 m and promise only slightly reduced accuracy for dynamic scenarios at distances of several hundred metres (Zogg and Maar, 2020; Grimm et al., 2015). Therefore, the introduction of RTS as an alternative, more accurate positioning sensor to GNSS for UAS geo-referencing can increase the accuracy of the UAS trajectory and, consequently, the accuracy of the collected geo-data.

In this study, we do not only show the calculation of a geo-referenced point cloud generated on a trajectory obtained from fusion of RTS and Inertial Measurement Unit (IMU) measurements but also focus on potential ways to evaluate such highly accurate trajectories. The high expected accuracy of an RTS-based trajectory makes the absolute evaluation challenging since no acquisition technique with superior accuracy is available. We use three independent approaches to evaluate the UAS trajectory measured by RTS (see Figure 1): (I) a camera mounted on the UAS captures images of a dense reference field in the flight area to allow the reconstruction of the camera position using photogrammetric resection, (II) a second RTS is used to gather redundant measurements of the UAS position, thus measuring an independent 3D trajectory of the same target, and (III) an additional data set uses the point cloud calculated using

the RTS/IMU-integrated trajectory and the ULS measurements and compares it with a reference point cloud obtained from terrestrial laser scanning (TLS). Consequently, our work aims to evaluate the results on the level of both the trajectory and the point cloud. Evaluation of the contribution of the individual system components is not within the scope of this paper.

This contribution starts with the presentation of relevant work in the field of RTS-based trajectory determination for UAS mapping (Section 2). After that, Section 3 describes the multisensor system used in our work, the study area and the three reference data sets on which we evaluate the observed UAS data. In Section 4 the results of the comparison and analysis of the data sets are shown followed by a discussion.

### 2. Related Work

The generation of a 3D point cloud of the environment with a multisensor system can be divided into two major steps. The first step is the estimation of the platform trajectory, traditionally achieved by fusing data from GNSS and IMU sensors (Pfeifer et al., 2012). The second step is the direct geo-referencing of the acquired images and/or laser data. Regarding trajectory estimation, modern RTS offer an alternative solution to geo-reference data from mobile mapping systems. Many studies use RTS to determine the trajectory of kinematic platforms. Kälin et al. (2022); Kerekes and Schwieger (2018); Thalmann and Neuner (2021); Tombrink et al. (2023) use RTS for time-synchronized measurements that allow the generation of highly accurate trajectory information. In Dammert et al. (2024) the uncertainty of UAS trajectories measured by RTS is investigated based on a Monte-Carlo simulation, building the preparatory work for this practical evaluation. Roberts and Boorer (2016) perform a field experiment using an older RTS model to measure UAS trajectories. However, their uncertainty evaluation lacks adequate data for comparison, the consideration of the lever arm between the camera mounted on the UAS and the measured prism, and an accurate time synchronization approach, leading to a concluded uncertainty of the RTS

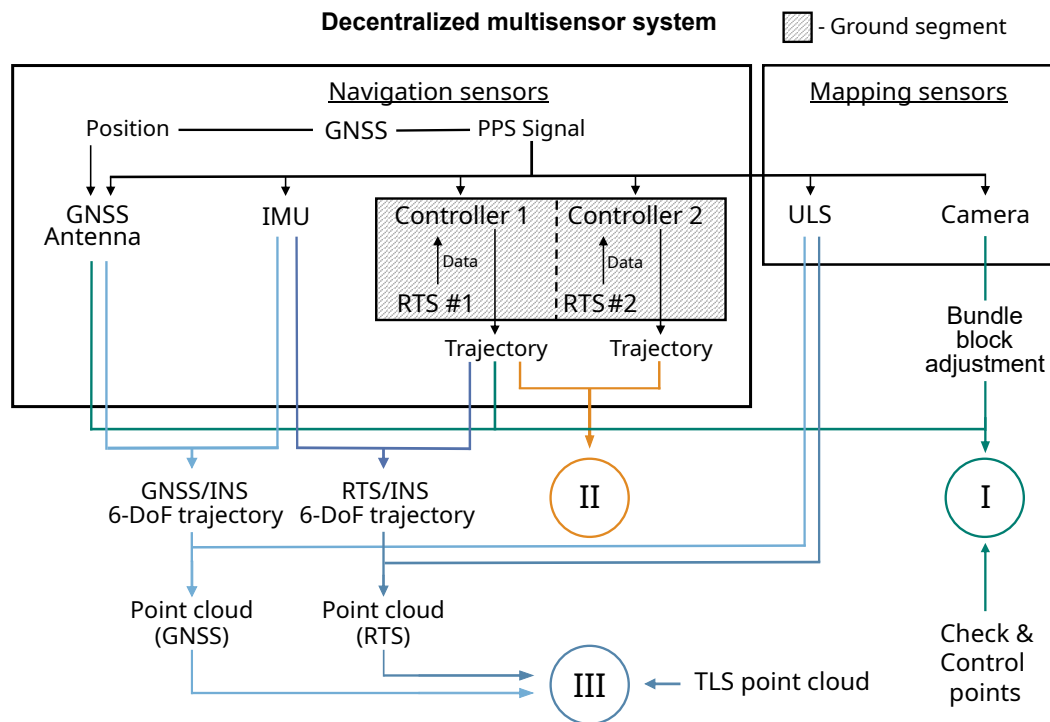


Figure 1. Concept of the decentralized sensor system and processing pipeline for data sets I, II and III. The grey box marks the ground segment, while the other sensors are mounted on the UAS.

measurement of about 20 cm. All these shortcomings are addressed in our contribution, while also using state-of-the-art instruments.

While traditional sensor fusion for UAS positioning combines GNSS and IMU data, RTS and IMU data can be integrated in a similar manner. Recent work on sensor fusion has focused on adjustment-based approaches. The adjustment-based framework for integration of GNSS, IMU and optionally LiDAR data developed in Pöppel et al. (2024) can be easily adapted to integrate RTS and IMU data in a loosely-coupled approach, replacing the GNSS data with RTS measurements. Thalmann and Neuner (2024) present a tightly-coupled Extended Kalman Filter, designed to use raw distance and angle measurements of RTS together with IMU data. This approach leverages the raw measurements of RTS and thus allows for a most complete stochastic model. Additionally, their approach is robust against outliers in the RTS polar observations.

For the application of a photogrammetric multisensor system Kersten and Lindstaedt (2022) describe the benefit of an accurate trajectory on the direct geo-referencing of aerial imagery data. In their study, the use of RTK-GNSS trajectories allows for the reduction of ground control points down to five points, due to the accurate initial trajectory estimate. Additionally, the bundle block adjustment (BBA) is significantly stabilized by the accurate trajectory leading to a better estimation of the camera's interior orientation. In the context of airborne LiDAR measurements, direct geo-referencing is the central step to get from the trajectory and laser scanner measurements to a 3D point cloud (Pfeifer et al., 2012). The position of the laser scanner serves as translational input in the equation, meaning that errors in the trajectory position appear in the same magnitude in the geo-referenced point cloud. Consequently, a more accurate trajectory leads to a more accurate point cloud, emphasizing

the potential of new, more accurate methods to determine the trajectory of LiDAR platforms.

### 3. Materials and Methods

The data set investigated in our study was acquired in Siegendorf, Austria in May 2024 at our dedicated UAS reference field. The measurement campaign lasted a whole day with temperatures ranging from 20°C to 28°C and mostly strong sunshine. During the measurements, the temperature profile was repeatedly measured to correct the RTS measurements for atmospheric refraction effects. Within our measurement campaign, several combinations of distance between RTS and UAS, flying height and speed have been tested, but in this study, we focus on a flight that was performed at 100 m height with a speed of 3 m s<sup>-1</sup>.

The combination of an RTS with an IMU and mapping sensors onboard an airborne platform forms a decentralized multisensor system as the RTS (*ground segment*), and the UAS (*kinematic segment*) are spatially separated. Apart from the geometric transformation between the ground segment and measurements performed by the airborne, kinematic segment, time synchronization is a crucial factor.

The subsystems used in this study and our concept for synchronizing, processing and evaluating the data are shown in Figure 1. The data used are aggregated into three data sets (I, II and III) which are further described in Sections 3.4 - 3.6. Our work builds on the findings of Thalmann and Neuner (2021) to allow precise time synchronization between both segments using the PPS (pulse per second) information of the received GNSS signal. The two RTS are positioned approximately 300 m (horizontal distance) away from the centre of the flight path (Figure 3).

### 3.1 Robotic total station

To allow the time-synchronized data acquisition with an RTS, the RTS measurements are managed using an external controller. In our study, a Leica MS60 was used, which allows the execution of continuous measurements based on the GeoCom interface. These measurements are requested and recorded by a Raspberry Pi 4 which simultaneously logs time information in the form of NMEA (National Maritime Electronics Association) and PPS signals from a connected uBlox LEA-6T GNSS receiver. The Leica MS60 can determine the position of the UAS with a measurement frequency of about 20 Hz, allowing for a dense trajectory observation. The necessary reflector, installed on the kinematic segment, is a Leica GRZ-122 360° prism (Figure 2). This enables the tracking and measurement of the UAS independent of its orientation. The cyclic errors of < 3 mm caused by this reflector (Lackner and Lienhart, 2016), are neglected for this study.

### 3.2 UAS

The UAS utilized for this study is based on a Hammer X8B heavy-lift RTF drone, customized by the companies Kopterworx and Skyability. This large platform enables the mounting of several measurement sensors and thus allows to capture a comprehensive data set. For our measurements, the UAS was equipped with the following measurement sensors:

- a Leica GRZ-122 360° prism as target for both RTS
- a RIEGL VUX-SYS airborne laser scanner with an Applanix AP-20 IMU
- a Sony Alpha 7R II camera

The sensors were mounted rigidly (see Figure 2) to allow the accurate transformation between the different data sets. The lever arms and misalignment angles within the rigid sensor mounting were determined by industrial surveying methods (laser tracker and connected laser scanner) in combination with our 3D camera calibration field.



Figure 2. Rigid mounting of a) 360° prism, b) RIEGL VUX-SYS including Applanix AP-20 and c) Sony Alpha 7R II on our UAS

### 3.3 Study area

Our study area in Siegendorf, Austria, consists of two orthogonal arms each with a length of 600 m, along which the RTS can be set up. On the intersection of those arms, the control point area is situated. There, a dense reference field was set up for the evaluation of the measured UAS trajectory based on photogrammetric data. The complete area with RTS positions, UAS trajectory and photogrammetric control points can be seen in Figure 3.

The control point area is approximately 120 m x 120 m and has about 100 re-mountable photogrammetric targets that can be used for a resection of the camera position. The 3D coordinates of all targets have been determined using static total station measurements, leading to a point uncertainty of < 3 mm. To

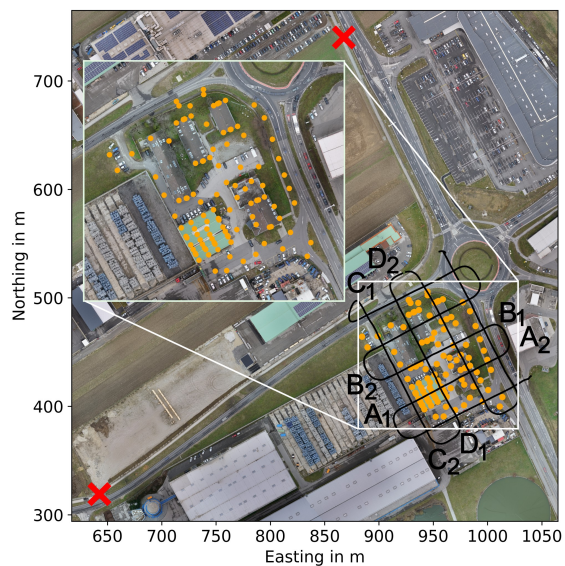


Figure 3. Study area with trajectory (black), RTS positions (red crosses) and distributed photogrammetric targets (orange). Flight strips used in Section 4.3 and their directions are denoted by letters A-D with the direction going from subscript 1 to 2.

also leverage the data acquired by the ULS, a reference point cloud of the central area was acquired using a Riegl VZ-400i terrestrial laser scanner. This point cloud has an RMSE of < 5 mm, assessed via checkpoints measured with a total station.

Both, the point cloud and the photogrammetric targets are connected to the RTS positions by geodetic network measurements. This guarantees an accurate coordinate frame in the study area and thus a reliable combination of RTS, camera, ULS and TLS measurements.

### 3.4 Bundle block adjustment of airborne imagery

The Sony Alpha 7R II mounted on the UAS captured 189 timestamped images along the trajectory, which forms a cross-flight pattern. For this data set, all images were captured at a height of 100 m above ground, resulting in a Ground Sampling Distance (GSD) of 18 mm. The images are processed using Agisoft Metashape, where 10 reference points were manually picked in all images and selected as control points to accurately geo-reference the bundle block. These points are evenly distributed over the study area and exhibit different elevations,

as half of these points are installed on buildings. Using the common time system of the image timestamps and the trajectory measured by the RTS, the trajectory is linearly interpolated on the camera timestamps. For the orientation of the images in the processing software, the RTS-derived UAS positions are then introduced as initial camera locations, establishing a workflow fully independent of GNSS positions. Within the bundle block adjustment, a camera position is then estimated for each image. Allowing the comparison of the estimated camera positions to the positions measured by the RTS, after considering the lever arm components. The comparison with the post-processed GNSS positions is performed in an identical manner, giving additionally the differences to the GNSS positions. This image-based data set is henceforth referred to as data set I.

### 3.5 Redundant trajectory of two RTS

RTS are one of the most accurate ways to determine the position of objects in outdoor environments. Therefore, the evaluation of RTS measurements by another sensor of higher quality in long-range, outdoor scenarios is challenging. Typical reference sensors, such as laser trackers (Vogel et al., 2023), optical tracking systems (Kälin et al., 2023) or robotic arms (Thalmann and Neuner, 2021), can not operate at the distances required for UAS tracking. A feasible solution is therefore the redundant measurement of the trajectory with a second RTS. In our work, we use the trajectory measured by a second RTS to evaluate the trajectory measurements of our first RTS. To compare both trajectories, the measurements of the second RTS are linearly interpolated onto the measurement timestamps of the first RTS. Due to the high measurement frequency of 20 Hz and a threshold of 100 ms above which potential data gaps are not filled by interpolation, the additional uncertainty introduced by interpolation is neglected in our study. While the same measurement principle is used, the RTS operate independently from another, enabling a redundant measurement of the trajectory. This independent measurement gives us an insight into the quality of the realization of the time base of the decentralized system components and the kinematic positioning. The redundant trajectory determination by two RTS forms our second data set (II).

### 3.6 Evaluation of directly geo-referenced point clouds

Another approach to evaluate the quality of the proposed method is the comparison of the resulting point cloud with a TLS reference point cloud. The point cloud to be evaluated is generated by direct geo-referencing of the ULS measurements using the RTS/IMU-integrated trajectory. This allows an independent assessment of the whole multisensor system. The identification of individual error contributions from the ULS, IMU, RTS and TLS however, is not possible. Consequently, this data set evaluates the quality of the obtained point cloud. Since the uncertainty of both the point cloud and the trajectory are of interest, this assessment of the absolute uncertainty of the acquired point cloud is of great value.

The RTS/IMU integration employed in this work is performed using a variation of the loosely-coupled adjustment algorithm described in Pöppel et al. (2024). The main difference is the replacement of GNSS position measurements with the RTS position measurements, with the covariance of the latter propagated from the underlying polar measurements. In this analysis, LiDAR correspondences are not used in order to focus solely on the RTS/IMU contribution to the point cloud. While the time

delay between RTS and IMU is largely corrected using the calibration procedure of Thalmann and Neuner (2021), a remaining constant latency is empirically estimated and applied prior to the RTS/IMU adjustment. The rationale for this approach is based on recent findings that the RTS exhibits an additional latency for outdoor scenarios, which we are not yet able to calibrate in our laboratory setup. Therefore, accounting for this by estimating a residual latency is a feasible solution. After the estimation of the RTS/IMU-integrated trajectory, the ULS data are directly geo-referenced. The resulting point cloud is then separated into individual strips and evaluated with reference to the TLS point cloud using normal distances derived by the M3C2 algorithm (Lague et al., 2013). For our evaluation, the absolute values of the normal distances are considered. Similar to data set I, an identical workflow is performed for the GNSS/IMU trajectory, allowing some context for the shown results. The results of the M3C2 comparisons for four flight strips (see Figure 3) build our third data set III.

## 4. Results and discussion

In the following part, the results of the data sets that were acquired during our measurement campaign and processed according to Section 3 are presented.

### 4.1 Trajectory differences to estimated camera positions

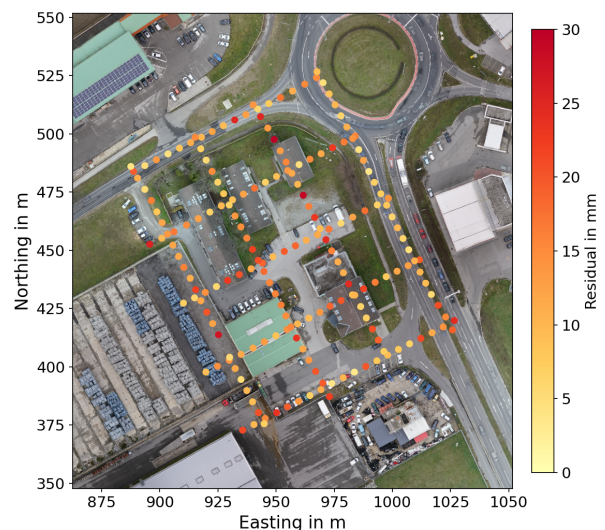


Figure 4. Residuals of trajectory measured by RTS #1 after bundle-block adjustment of 189 images

Figure 4 and Figure 5 show the residuals of the estimated camera positions with reference to the RTS-measured positions. The latter are used as input in the BBA. The BBA uses 10 ground control points (GCP), which have a stated 3D error of  $< 5$  mm after the BBA. This is significantly lower than the GSD of the used camera and only slightly higher than the standard deviation of our reference coordinates ( $< 3$  mm). The 3D residuals of the camera positions (Figure 4 and Figure 5), range from 3 mm to 33 mm with a mean value of 13 mm and an RMSE of 6 mm. The decomposition of the residuals into their components shows that the dominant influence is along the horizontal plane with a mean error of 11 mm and an RMSE of 6 mm. The workflow described in Section 3.4 is also performed using the GNSS trajectory, to allow the interpretation of the RTS residuals relative to the GNSS residuals. The histograms of the 3D

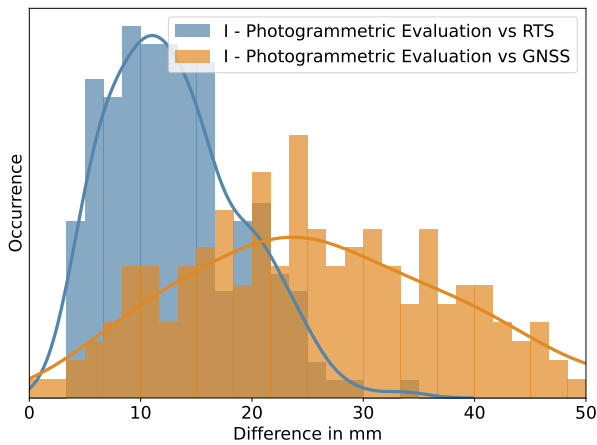


Figure 5. Residuals of trajectory measured by RTS #1 (blue) and GNSS (orange) after bundle-block adjustment of 189 images

residuals are shown in Figure 5. The plot reveals that the residuals of the camera positions measured by GNSS show a higher mean value of 27 mm and a larger spread with an RMSE of 14 mm than the evaluation against the RTS positions.

#### 4.2 Comparison of redundant RTS trajectories

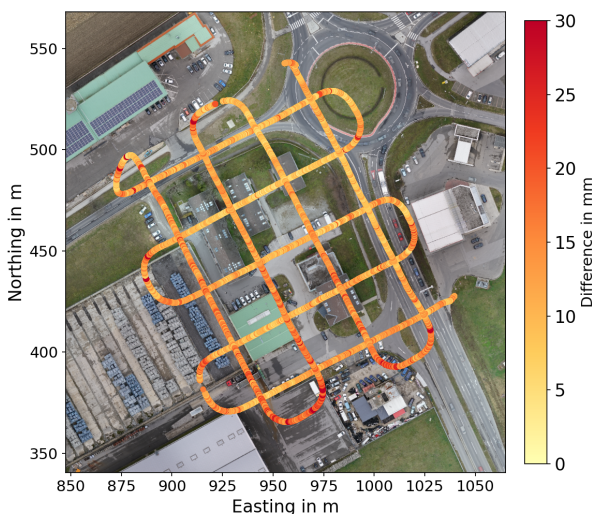


Figure 6. 3D Differences between trajectories measured by RTS #1 and RTS #2

Figure 6 shows the 3D differences between the trajectory derived from RTS #1 and RTS #2, respectively. The differences range up to 23 mm with 90% of the values smaller than 17 mm. The mean difference is 11 mm with an RMSE of 4 mm. However, the spatial distribution of the differences is not homogeneous and the southeast parts of the trajectory, which are most distant from both RTS, show the highest values. Additionally, the turning parts of the trajectory exhibit higher values in general but in particular extremely high values for short periods of time.

#### 4.3 Strip-wise distances to reference point cloud

In this evaluation, we compare the point clouds of individual flight strips, directly geo-referenced with the trajectories from

either RTS/IMU or GNSS/IMU, to our TLS reference point cloud. Due to the large influence of the high-end IMU data in the sensor integration, the RTS/IMU and GNSS/IMU integrated trajectories differ only by a maximum value of 15 mm, with a mean difference of about 7 mm. For the point cloud comparison, we only consider open, non-vegetated areas. Figure 7 shows the point cloud and its absolute M3C2 differences obtained from RTS/IMU for strip A. The resulting distributions of the absolute normal distances from the M3C2 comparison are shown in Figure 8 for four separate flight strips (A to D), the positions of these strips are shown in Figure 3. The violin plots also show the calculated quartiles of the distributions (dashed lines).

For strips A and B, the GNSS-derived point clouds are significantly worse than the RTS-derived point clouds. The large deviations show an overall poorer performance for the GNSS-derived point cloud. The absolute M3C2 distances based on the RTS-derived point cloud show an expected distribution. For strip C the results of GNSS and RTS are quite similar, showing a significantly better result of the GNSS data. There, the GNSS slightly outperforms the RTS solution. However, strip D shows again the large fluctuation of the GNSS-derived point clouds as the result is again worse than the RTS solution. The shape of the distribution for strips C and D for the GNSS is much closer to the ideal distribution than for strips A and B. However, the RTS shows closeness to the expected distribution for all strips and exhibits consistently low values for the normal distance. In summary, the mean value for GNSS ranges from 8 mm to 21 mm, with a maximum 90th-percentile of 45 mm. For the RTS-derived point clouds, the corresponding values are all smaller with mean deviations in the range of 8-10 mm and maximum 90th-percentile of 19 mm.

#### 4.4 Discussion

The results shown in Sections 4.1 and 4.2 show similar differences towards the trajectory determined using RTS (see also Table 1). The differences of data set I (Section 4.1) to the GNSS positions are considerably larger than to the RTS positions. The comparison of both trajectories to the camera positions estimated by BBA (data set I) shows large differences between RTS and GNSS. The mean value as well as the RMSE of the RTS-determined camera positions show a much better performance than the GNSS-determined camera positions. While the evaluation result includes the uncertainty of the photogrammetric estimation of the camera poses, this uncertainty affects the RTS and GNSS to a similar magnitude. The average difference and the spread of the distribution obtained from RTS are better than the GNSS metrics by a factor of two. In general, the differences calculated for the GNSS lie in the expected uncertainty range of a few centimetres for post-processed GNSS trajectories.

For data set II, the differences between the trajectories measured by RTS #1 and RTS #2 show short-timed peaks which appear in particular in the turning parts of the trajectory. These peaks originate in the partial obstruction of the line-of-sight between RTS and the reflector due to the landing gear of the UAS. Although the effect of this obstruction on the overall trajectory is quite small, as it appears only in the turns and there only for short periods, we will improve the setup accordingly. Data set II also shows an increasing difference between both trajectories for increasing distances between the UAS and the RTS (southeast area). Since many uncertainties of RTS measurements (angle measurement uncertainties, atmospheric effects, etc.) increase with higher distances, this effect is expected. In general, the discrepancies of the redundant trajec-

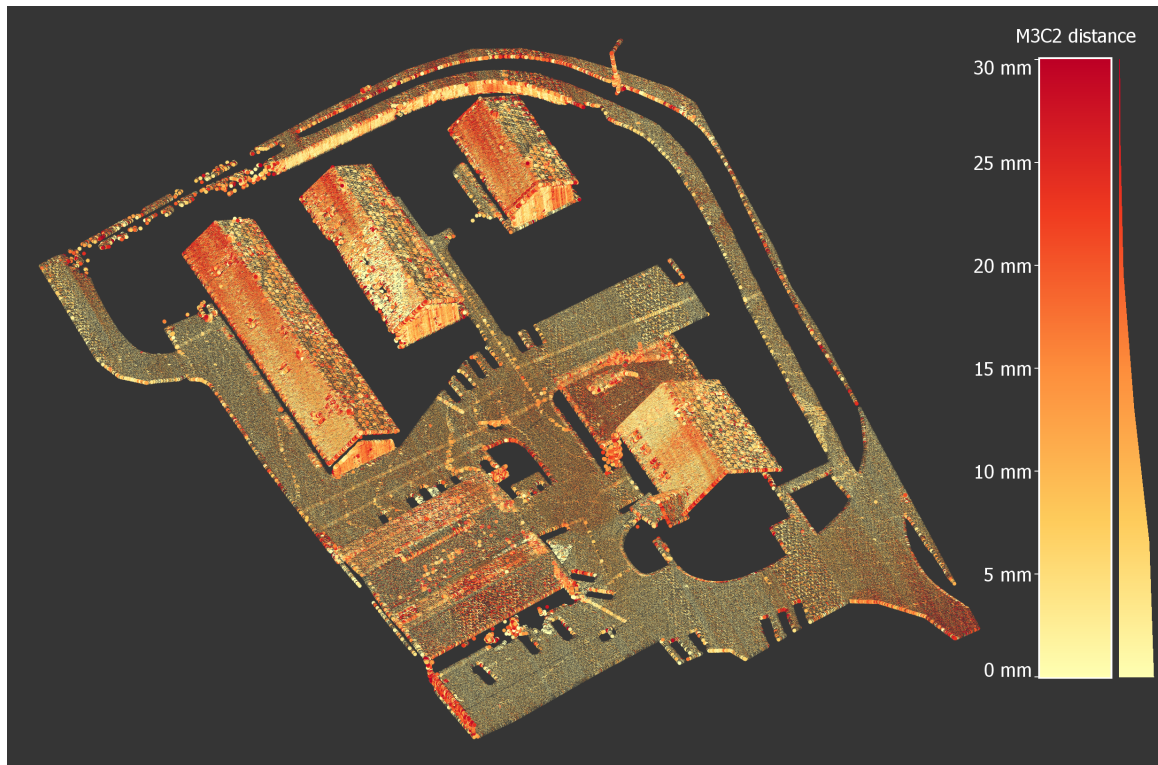


Figure 7. Point cloud of the study area, filtered for non-vegetated areas, calculated using RTS/IMU integration for strip A. The colourization is according to the absolute normal distances to the TLS point cloud

Data set	Sensor	Vertical		Horizontal		3D	
		Mean Difference	RMSE	Mean Difference	RMSE	Mean Difference	RMSE
I	RTS	5 mm	4 mm	11 mm	6 mm	13 mm	6 mm
I	GNSS	13 mm	9 mm	21 mm	14 mm	27 mm	14 mm
II	RTS	7 mm	4 mm	8 mm	4 mm	11 mm	4 mm
III	RTS	-	-	-	-	9 mm	8 mm
III	GNSS	-	-	-	-	14 mm	12 mm

Table 1. Evaluation of data sets I and II split into vertical and horizontal components of the differences, data set III shows only the absolute normal distances

ory determination by a second RTS show similar deviations as the comparison to the photogrammetric estimation of camera poses. Both show mean differences of 11 mm and 13 mm (Table 1) respectively. The high agreement of data sets I and II confirms that the uncertainty of the trajectory measured by RTS is even lower than the reported difference values, as the differences are a result of the uncertainty of the RTS and the compared sensor. However, quantifying the exact contribution of each sensor in this difference is beyond the scope of this paper.

The differences reported in Section 4.3 reach comparable magnitudes for the point cloud differences as for the trajectory comparisons of Sections 4.1- 4.2. While the point cloud differences include additional error sources compared to the RTS trajectory, which would increase the exhibited uncertainties, the integration of the IMU data can also improve the trajectory. In our fieldwork, a high-accuracy IMU was used which, in combination with the rather short flight times, leads to an improvement of the RTS trajectory due to the fusion of the sensors. Consequently, the point cloud differences do not exhibit much larger deviations from our reference data than the trajectory-based evaluations. In general, this fact hinders a pure comparison between the point clouds generated using either RTS or

GNSS as positioning sensor, because the strong influence of the IMU improves both trajectories. Due to the lower accuracy of GNSS, the GNSS/IMU-integrated trajectory benefits more from the accurate IMU measurements than the RTS/IMU-integrated trajectory. The point cloud differences compared to the TLS reference show that the point cloud determined using RTS/IMU integration (i) is more consistent with our TLS reference for the evaluated strips than the GNSS/IMU-based point cloud (ii). Apart from the lower overall values, (i) exhibits consistent values for the mean differences and the 90th percentiles. For (ii), the values of the 90th-percentiles vary in the range of several centimetres. Even though for strip C, (ii) achieves an accuracy similar to (i), the large variation of (ii) between the different strips marks the good result of strip C an exception. Therefore, (i) outperforms (ii) showing that RTS/IMU-based point clouds allow for more consistent and accurate results.

In general, data set I allows us to conclude that our RTS-measured trajectory is about two times more consistent with our reference than the GNSS-based trajectory determination. Together with data set II, a statement can be made that the UAS position determined by RTS #1 agrees to 13 mm (Photogrammetry) and 11 mm (RTS #2), respectively, with our redundant trajectory measurements. Data set III shows that the RTS/IMU

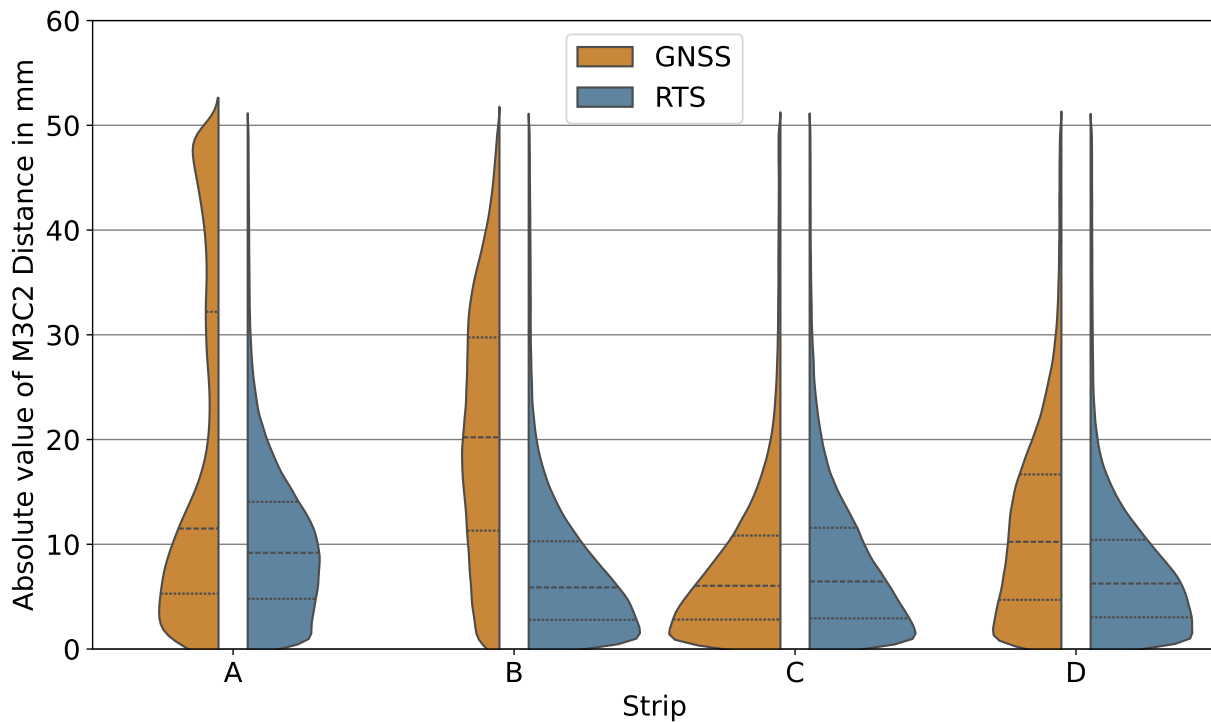


Figure 8. Violin-Plots for each strip, showing the distribution of differences between GNSS/IMU-based point cloud and TLS (orange) and RTS/IMU-based point cloud and TLS (blue). The dashed lines show the quartiles

integration for the generation of point clouds provides consistent results with the TLS reference for all evaluated strips, while the GNSS/IMU integration shows higher deviations for most strips.

For this study, it is worth mentioning that the study area provides optimal operation conditions for GNSS (flat, open-sky environment). On the other hand, the summerly weather increased turbulence in the lower atmosphere, decreasing the accuracy of the RTS measurements. Considering this, the results might vary for different operating conditions.

#### 4.5 Outlook

In our ongoing work, we aim to further analyse the uncertainty budget of RTS-determined trajectories and identify the main components, using simulations and sensitivity analysis. We also aim to put a special emphasis on how larger distances influence the measurement uncertainty and which constraints are required to allow millimetre-level uncertainties. Additionally, we develop a calibration model to minimize systematic errors caused by the geometry of the used reflector for our application, potentially allowing the improvement of the RTS measurements by several millimetres. For this, we will perform additional field campaigns in our study area, and (step-by-step) improve the performance of trajectory measurements with RTS.

### 5. Conclusion

In our study, we present an extensive field campaign aimed at investigating the trajectory determination of UAS with robotic total stations (RTS). Combined with IMU measurements, we create a geo-referenced 3D point cloud using only RTS, IMU and ULS data. Thus, we completely replace the GNSS positioning of the UAS. We present three different data sets suitable

for the evaluation. Data set I uses a photogrammetric sensor and II a redundant trajectory determination by a second RTS to evaluate the measured trajectory. The generated point cloud is compared against a ground truth TLS reference point cloud in data set III. Data sets I and III are also compared against the GNSS observed trajectory to put the results for the RTS-measured trajectory into a meaningful context.

For the RTS, the 3D trajectory discrepancies of data sets I and II show, on average, values of 13 mm and 11 mm, respectively, hinting at a trajectory uncertainty of the RTS measurements smaller than this value. We reason this by the fact that the uncertainty of the reference data sets smears the uncertainty of the trajectory measured by the RTS. For data set I, GNSS shows a mean discrepancy of 27 mm with a significantly larger spread of the values. Therefore, the RTS achieves results about two times more consistent with our photogrammetric reference than the GNSS data. Using the RTS/IMU-integrated trajectory, data set III exhibits a mean absolute M3C2 distance to our TLS reference data of 9 mm. The evaluation of data set III based on the GNSS/IMU trajectory shows a mean value of 14 mm, which accounts for an increase of 55% compared to the RTS/IMU-based point cloud. Additionally, the individual strips evaluated in data set III vary greatly for the GNSS evaluation, while the RTS evaluation shows consistent distributions with overall lower results for the differences from the reference data set.

Overall, our work shows a successful pipeline to generate 3D point clouds from trajectories determined using RTS and IMU. The high accuracy of RTS-measured trajectories is shown for all three data sets, and the increased accuracy compared to GNSS-measured trajectories is shown in data sets I and III. However, the presented method has certain constraints. The line of sight between the RTS and UAS must remain unobstructed, and the maximum distance between them should not exceed 500 m to ensure reliable and accurate measurements, as the un-

certainty increases with greater distances. Thus, the RTS-based trajectory acquisition is most suited for high-accuracy, small-scale scenarios. Additionally, transforming the locally measured UAS trajectory into a global coordinate frame requires supplementary measurements, such as GNSS observations.

## 6. Acknowledgments

This research was conducted under the *TrackDrone* project (Grant No. 895310) funded by the Austrian Research Promotion Agency (FFG).

## References

- Dammert, L., Monetti, D., Thalmann, T., Neuner, H.-B., Mandlbürger, G., 2024. Simulation based analysis of high precision uav tracking with robotic total stations. *DGPF-Jahrestagung 2024 - Stadt, Land, Fluss - Daten vernetzen*, Stuttgart, 203–210. Geschäftsstelle der DGPF, doi: <https://doi.org/10.24407/KXP:1885662106>.
- Grimm, D., Kleemaier, G., Zogg, H.-M., 2015. ATRplus White Paper. Leica Geosystems AG.
- Kerekes, G., Schwieger, V., 2018. Kinematic positioning in a real time robotic total station network system. *Proceedings of 6th international conference on machine control & guidance*, 35–43.
- Kersten, T., Lindstaedt, M., 2022. UAV-basierte Bildflüge mit RTK-GNSS - brauchen wir da noch Passpunkte? *UAV 2022 – Innovation und Praxis, Schriftenreihe des DVW, Band 100*.
- Kälin, U., Hürzeler, M., Grimm, D., 2023. Calibration of Kinematic Measuring Systems. *Ingenieurvermessung 23. Beiträge zum 20. Internationalen Ingenieurvermessungskurs Zürich, 2023*, 195–207. Wichmann.
- Kälin, U., Staffa, L., Grimm, D. E., Wendt, A., 2022. Highly Accurate Pose Estimation as a Reference for Autonomous Vehicles in Near-Range Scenarios. *Remote Sensing*, 14(1), 90. Number: 1 Multidisciplinary Digital Publishing Institute, doi: <https://doi.org/0.3390/rs14010090>.
- Lackner, S., Lienhart, W., 2016. Impact of Prism Type and Prism Orientation on the Accuracy of Automated Total Station Measurements. *Proc. Joint International Symposium on Deformation Monitoring (JISDM)*, 8.
- Lague, D., Brodu, N., Leroux, J., 2013. Accurate 3D comparison of complex topography with terrestrial laser scanner: Application to the Rangitikei canyon (NZ). *ISPRS journal of photogrammetry and remote sensing*, 82, 10–26.
- Paraforos, D. S., Reutemann, M., Sharipov, G., Werner, R., Griepentrog, H. W., 2017. Total station data assessment using an industrial robotic arm for dynamic 3D in-field positioning with sub-centimetre accuracy. *Computers and Electronics in Agriculture*, 136, 166–175. Elsevier B.V., doi: [10.1016/j.compag.2017.03.009](https://doi.org/10.1016/j.compag.2017.03.009).
- Pfeifer, N., Glira, P., Briese, C., 2012. Direct georeferencing with on board navigation components of light weight UAV platforms. *The International Archives of the Photogrammetry, Remote Sensing and Spatial Information Sciences*, 39, 487–492. Copernicus GmbH, doi: <https://doi.org/10.5194/isprsarchives-XXXIX-B7-487-2012>.
- Pöpl, F., Ullrich, A., Mandlbürger, G., Pfeifer, N., 2024. A flexible trajectory estimation methodology for kinematic laser scanning. *ISPRS Journal of Photogrammetry and Remote Sensing*, 215, 62–79. Elsevier B.V., doi: <https://doi.org/10.1016/j.isprsjprs.2024.06.014>.
- Roberts, C., Boorer, P., 2016. Kinematic positioning using a robotic total station as applied to small-scale UAVs. *Journal of Spatial Science*, 61(1), 29–45. Taylor & Francis, doi: <https://doi.org/10.1080/14498596.2015.1068232>.
- Thalmann, T., Neuner, H., 2021. Temporal calibration and synchronization of robotic total stations for kinematic multi-sensor-systems. *Journal of Applied Geodesy*, 15(1), 13–30. De Gruyter, doi: <https://doi.org/10.1515/jag-2019-0070>.
- Thalmann, T., Neuner, H., 2024. Sensor fusion of robotic total station and inertial navigation system for 6DoF tracking applications. *Applied Geomatics*. Springer, doi: <https://doi.org/10.1007/s12518-024-00593-4>.
- Tombrink, G., Dreier, A., Klingbeil, L., Kuhlmann, H., 2023. Trajectory evaluation using repeated rail-bound measurements. *Journal of Applied Geodesy*, 17(3), 205–216. De Gruyter, doi: <https://doi.org/10.1515/jag-2022-0027>.
- Vaidis, M., Dubois, W., Daum, E., LaRocque, D., Pomerleau, F., 2023. Uncertainty analysis for accurate ground truth trajectories with robotic total stations. *2023 IEEE/RSJ International Conference on Intelligent Robots and Systems (IROS)*. IEEE, doi: <https://doi.org/10.48550/arXiv.2308.01553>.
- Vogel, S., van der Linde, M., Hake, F., 2023. Development and Validation of an External GPS Time Synchronization for Robotic Total Station Control. *Ingenieurvermessung 23. Beiträge zum 20. Internationalen Ingenieurvermessungskurs Zürich, 2023*, 181–194. Wichmann.
- Zogg, H.-M., Maar, H., 2020. Leica Nova MS60 White Paper. Leica Geosystems AG.